



NRL/MR/6410--06-8943

A Brief Note on Implementing Boundary Conditions at a Solid Wall Using the FCT Algorithm

JUNHUI LIU

CAROLYN R. KAPLAN

*Center for Reactive Flow and Dynamical Systems
Laboratory for Computational Physics and Fluid Dynamics*

ELAINE S. ORAN

*Senior Scientist for Reactive Flow Physics
Laboratory for Computational Physics and Fluid Dynamics*

April 7, 2006

20060425232

REPORT DOCUMENTATION PAGE				Form Approved OMB No. 0704-0188	
Public reporting burden for this collection of information is estimated to average 1 hour per response, including the time for reviewing instructions, searching existing data sources, gathering and maintaining the data needed, and completing and reviewing this collection of information. Send comments regarding this burden estimate or any other aspect of this collection of information, including suggestions for reducing this burden to Department of Defense, Washington Headquarters Services, Directorate for Information Operations and Reports (0704-0188), 1215 Jefferson Davis Highway, Suite 1204, Arlington, VA 22202-4302. Respondents should be aware that notwithstanding any other provision of law, no person shall be subject to any penalty for failing to comply with a collection of information if it does not display a currently valid OMB control number. PLEASE DO NOT RETURN YOUR FORM TO THE ABOVE ADDRESS.					
1. REPORT DATE (DD-MM-YYYY) 07-04-2006		2. REPORT TYPE Memorandum Report		3. DATES COVERED (From - To)	
4. TITLE AND SUBTITLE A Brief Note on Implementing Boundary Conditions at a Solid Wall Using the FCT Algorithm				5a. CONTRACT NUMBER	
				5b. GRANT NUMBER 64-1530-0-6	
				5c. PROGRAM ELEMENT NUMBER	
6. AUTHOR(S) Junhui Liu, Carolyn R. Kaplan, and Elaine S. Oran				5d. PROJECT NUMBER	
				5e. TASK NUMBER	
				5f. WORK UNIT NUMBER	
7. PERFORMING ORGANIZATION NAME(S) AND ADDRESS(ES) Naval Research Laboratory 4555 Overlook Avenue, SW Washington, DC 20375-5320				8. PERFORMING ORGANIZATION REPORT NUMBER NRL/MR/6410--06-8943	
9. SPONSORING / MONITORING AGENCY NAME(S) AND ADDRESS(ES)				10. SPONSOR / MONITOR'S ACRONYM(S)	
				11. SPONSOR / MONITOR'S REPORT NUMBER(S)	
12. DISTRIBUTION / AVAILABILITY STATEMENT Approved for public release; distribution is unlimited.					
13. SUPPLEMENTARY NOTES					
14. ABSTRACT The implementation of boundary conditions at a solid wall using the flux-corrected transport (FCT) algorithm has been studied. We found that extrapolating the interior points to obtain the pressure at the wall may introduce instability. Instead, the given physical conditions at the wall, such as the continuity equation and the given thermal conditions, should be used to evaluate the pressure at the wall. Since the viscous diffusion and other source terms can be calculated from flow variables at interior points and the wall surface, the need to specify the guard-cell values at a solid wall is only required by the numerical diffusion embedded in FCT. Guard-cell values may interfere with the activation of the flux limiter near the wall, introducing either numerical instability or producing unphysical numerical results. Several approaches have been proposed to control this interference, such as turning off numerical diffusion at the first cell near the wall, or introducing extra numerical diffusion in the momentum equation at the wall to suppress the instability.					
15. SUBJECT TERMS Compressible flow Boundary-layer flow Numerical diffusion Flux-corrected transport Boundary conditions Flux limiter					
16. SECURITY CLASSIFICATION OF:			17. LIMITATION OF ABSTRACT UL	18. NUMBER OF PAGES 21	19a. NAME OF RESPONSIBLE PERSON Junhui Liu
a. REPORT Unclassified	b. ABSTRACT Unclassified	c. THIS PAGE Unclassified			19b. TELEPHONE NUMBER (include area code) (202) 767-6590

Contents

1. Introduction	1
2. FCT Algorithm	2
3. Implementing boundary conditions at a solid wall	3
(a) Evaluation of the wall pressure	4
(b) Density and energy in the guard cells	5
(c) Interference between the guard-cell values and the flux limiter	6
4. Numerical Results	8
5. Conclusions	11
6. Acknowledgments	11
References	12

A BRIEF NOTE ON IMPLEMENTING BOUNDARY CONDITIONS AT A SOLID WALL USING THE FCT ALGORITHM

1. Introduction

Early implementation of the flux-corrected transport (FCT) algorithms in Navier-Stokes codes has found that the boundary condition at a solid wall is susceptible to numerical instability when the temporal variation of the density near a wall is not small [1, 2]. This can occur in a simulation of an unsteady flow or in the initial stages of a steady-state simulation. In their numerical simulation of shock bifurcation near the end wall of a shock tube, Weber et al. [1] attributed the oscillations near the wall to the clipping of the density minimum by the FCT flux limiter, which is activated at locations where minima and maxima are present. They thus turned off the flux limiter in the immediate neighborhood of the density minimum to control the numerical oscillations temporarily. Saint-Martine-Tillet and Oran [2], on the other hand, used the local one-dimensional inviscid relations (LODI) developed by Poinso and Lele [3] to implement wall boundary conditions in a subsonic channel flow with ribs.

LODI has been developed by adopting the inviscid characteristic analysis to the Navier-Stokes equations [3], and has gained much attention in the implementation of boundary conditions. Although LODI maybe applicable to inflow, outflow and farfield boundaries [4], it is in conflict with the physical conditions at the wall when the normal pressure gradient at the wall is not small.

In this note, we discuss a different approach that uses the continuity and momentum equations, rather than the inviscid characteristic analysis, to define boundary conditions at the wall. Because the flow equations are used at the wall boundary, boundary conditions defined in this way are consistent with the conditions used by interior points. We have also found that this approach is more stable than LODI.

2. FCT Algorithm

We begin with a one-dimensional convection equation with source terms:

$$\frac{\partial \Phi}{\partial t} + \frac{\partial \Phi v}{\partial y} = -c_1 \frac{\partial P}{\partial y} + c_2, \quad (1)$$

where v is the local convection velocity, and P is the pressure-type variable. The quantity Φ can be any flow variable, such as density ρ , momentum fluxes $(\rho u, \rho v, \rho w)$, or energy E . Values of c_1 and c_2 can be constant or functions of convected variables. The application of FCT to this type of equation consists of three steps [5, 6]:

(1) Central difference the convection terms:

$$\Phi_j^T = \Phi_j^o - \frac{1}{2} [\epsilon_{j+\frac{1}{2}} (\Phi_{j+1}^o + \Phi_j^o) - \epsilon_{j-\frac{1}{2}} (\Phi_j^o + \Phi_{j-1}^o)] + c_1 \frac{\Delta t}{\Delta y} (P_{j+\frac{1}{2}} - P_{j-\frac{1}{2}}) + c_2 \Delta t, \quad (2)$$

where $\epsilon_{j+\frac{1}{2}} = v_{j+\frac{1}{2}} \frac{\Delta t}{\Delta y}$ is the local Courant number. The quantity Δy is the grid size and Δt is the time step. The subscript j is the center of a computational cell in the y direction. Superscript o denotes the quantity at time step $n-1$, and superscript T represents results at the next time level without adding numerical diffusion. A uniform grid is assumed for simplicity.

(2) Add numerical diffusion to stabilize the algorithm:

$$\tilde{\Phi}_j = \Phi_j^T + \nu_{j+\frac{1}{2}}^f (\Phi_{j+1}^o - \Phi_j^o) - \nu_{j-\frac{1}{2}}^f (\Phi_j^o - \Phi_{j-1}^o). \quad (3)$$

(3) Add antidiffusion to control the amount of numerical diffusion:

$$\Phi_j^n = \tilde{\Phi}_j - \mu_{j+\frac{1}{2}}^f (\Phi_{j+1}^T - \Phi_j^T) + \mu_{j-\frac{1}{2}}^f (\Phi_j^T - \Phi_{j-1}^T), \quad (4)$$

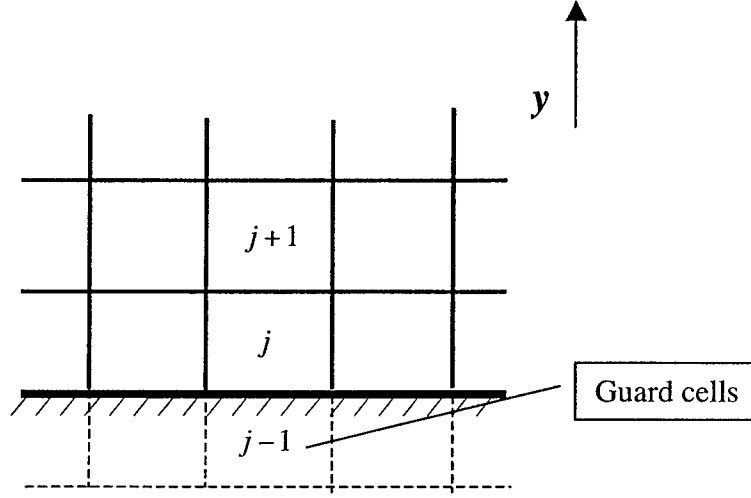
where quantities ν^f and μ^f are the added diffusion and antidiffusion coefficients, which are defined as

$$\begin{aligned} \nu^f &= \frac{1}{6} + \frac{\epsilon^2}{3}, \\ \mu^f &= D_c \left(\frac{1}{6} - \frac{\epsilon^2}{6} \right). \end{aligned} \quad (5)$$

The parameter D_c controls the amount of antidiffusion [8]. $D_c = 1.0$ corresponds to the minimum global numerical diffusion [8].

A flux-limiting technique is used in the third stage to assure the monotonicity of the solution by adjusting the amount of antidiffusion to avoid the generation of new maxima or minima in the solution. If a time-step splitting method is used [6], ϵ is evaluated at the time level $n + \frac{1}{2}$, for which an extra predictor step is needed to obtain ϵ at this time level.

3. Implementing boundary conditions at a solid wall



For a solid wall boundary shown in the sketch above, we need to specify boundary conditions for the following quantities:

- Values at the wall surface: $P_{j-\frac{1}{2}}$, $\epsilon_{j-\frac{1}{2}}$, $\mu_{j-\frac{1}{2}}^f$, and $\nu_{j-\frac{1}{2}}^f$
- Values in the guard cells: Φ_{j-1}^o and Φ_{j-1}^T

Here the subscript $j - \frac{1}{2}$ denotes the values at the wall surface. The Courant number $\epsilon_{j-\frac{1}{2}}$ is zero because of the no-slip conditions for a stationary wall, and the diffusion coefficient $\nu_{j-\frac{1}{2}}^f$ and the antidiffusion coefficient $\mu_{j-\frac{1}{2}}^f$ can be calculated from the equation (5). The other quantities to be defined are the pressure at the wall, $P_{j-\frac{1}{2}}$, and the convected variables in the guard cells, Φ_{j-1}^o and Φ_{j-1}^T . Because the difference between Φ_{j-1}^o and Φ_{j-1}^T consists only of the added numerical diffusion, they are specified similarly at boundaries. The choices

for Φ in a three-dimensional flow are $(\rho, \rho u, \rho v, \rho w, E)$, and the guard-cell values for the momentum fluxes at a no-slip, stationary wall can be specified as

$$\begin{aligned}(\rho u)_G &= -(\rho u)_L, \\(\rho v)_G &= -(\rho v)_L, \\(\rho w)_G &= -(\rho w)_L,\end{aligned}\tag{6}$$

where L is the cell adjacent to the wall, and G denotes the guard cell. The remaining quantities to be defined are the pressure at the wall and the density and energy in guard cells.

3.1. Evaluation of the wall pressure

We start with the continuity and the momentum equations at the wall:

$$\left. \frac{\partial \rho}{\partial t} \right|_W + \rho_W \left. \frac{\partial v}{\partial y} \right|_W = 0,\tag{7}$$

and

$$\left(\frac{\partial P}{\partial y} \right)_W = \left(\mu \frac{\partial^2 v}{\partial^2 y} \right)_W,\tag{8}$$

where quantity v is the velocity normal to the wall, the subscript “ W ” denotes the wall boundary, and ρ_W is the density at the wall. Equation (8) is a simplified version of the momentum equation at the wall for a compressible flow, assuming that the pressure gradient in the normal direction is mainly balanced by the normal viscous diffusion.

If the temporal variation of the density at the wall is negligible, the variations of the normal velocity v and the pressure gradient in the normal direction can be also ignored at the wall. Thus, a zero-pressure gradient can be assumed at the wall, and a simple extrapolation from the interior points can be used to obtain the wall pressure:

$$P_W = P_L.\tag{9}$$

On the other hand, if the temporal variation of ρ_W is not small, the normal velocity gradient and the pressure gradient near the wall can not be ignored. This is the case, for example, in a simulation of an unsteady flow or in a simulation of a steady-state flow with a rapidly

changing density in the initial stage. Equation (9) could result in numerical instability because of the inconsistency between a zero-pressure gradient used at the wall and that used by the interior points. Thus, physical conditions at the wall should be used to provide a consistent evaluation. The available conditions are the continuity equation (7), the momentum equation (8), and the given thermal conditions. The density at the wall, ρ_W , can be first evaluated from the continuity equation (7), and the wall pressure P_W can be calculated afterwards from this newly calculated ρ_W and the given thermal conditions, such as $P_W = \rho_W R T_W$ for an isothermal wall or $\frac{\partial P/\rho}{\partial y}\bigg|_W = 0$ for an adiabatic wall.

Following the LODI approach proposed by Poinso and Lele [3] and assuming $y = 0$ is the wall boundary, the equation calculating ρ_W in their approach would be

$$\frac{\partial \rho}{\partial t}\bigg|_W + \rho_W \frac{\partial v}{\partial y}\bigg|_W = \frac{1}{a_W} \frac{\partial P}{\partial z}\bigg|_W, \quad (10)$$

where a_W is the sound speed at the wall. The equation (10) is identical to the equation (7) if $\frac{\partial P}{\partial z}\bigg|_W = 0$. If $\frac{\partial P}{\partial z}\bigg|_W \neq 0$, however, the LODI approach would give an unphysical ρ_W , since the continuity equation is not satisfied at the wall.

3.2. Density and energy in the guard cells

Since the density, velocity and the thermal conditions are known at the wall, the pressure gradient and viscous diffusion can be evaluated from the flow variables at interior points and those at the wall. Thus, the specification of the guard-cell values only affects the numerical diffusion embedded in FCT at a stationary wall, as shown in equations (2)-(4).

If the wall is adiabatic and stationary, density and energy in the guard cells can be calculated from the pressure gradient at the wall, such as

$$\begin{aligned} \frac{\partial \rho}{\partial y}\bigg|_W &= \frac{1}{R T_W} \frac{\partial P}{\partial y}\bigg|_W \quad \text{and} \\ \frac{\partial E}{\partial y}\bigg|_W &= \frac{1}{\gamma - 1} \frac{\partial P}{\partial y}\bigg|_W, \end{aligned} \quad (11)$$

where $\frac{\partial P}{\partial y}\bigg|_W$ can be calculated from either the momentum equation (8) or a given value if

it is known beforehand. It should be mentioned that the relationship between the energy gradient and the pressure gradient given by equation (11) is also valid for other thermal conditions, such as an isothermal wall.

For an isothermal wall, the density and the energy are extrapolated from the values at the wall and those of the interior points, such as

$$\begin{aligned}\rho_G &= 2\rho_W - \rho_L \\ E_G &= 2E_W - E_L,\end{aligned}\tag{12}$$

where $E_W = P_W/(\gamma - 1)$.

3.3. Interference between the guard-cell values and the flux limiter

The numerical diffusion in FCT includes a global and a local component [8]. The global numerical diffusion is similar to viscous diffusion and its magnitude can be reduced to a very small value by adjusting the parameter D_c in equation (5). On the other hand, the local numerical diffusion, introduced by activating the flux limiter, varies spatially and intermittently. Furthermore, its magnitude is large and can be significantly larger than that of viscous diffusion. Guard-cell values may interfere with the flux limiter by activating the flux limiter in some unwanted regions, or by introducing a contradictory activation of the flux limiter for each variable.

Although the energy gradient given by equation (11) also applies at an isothermal wall, we have found that the temperature profile has an inflexion point near the wall if this equation, rather than the equation (12), is used to evaluate the energy in the guard cells. As we have discussed above, the guard-cell values only affect numerical diffusion at a stationary wall, this unwanted inflexion point should result from the interference between the guard-cell values and the numerical diffusion, or more specifically the flux limiter, since the magnitude of the local component of the numerical diffusion is significantly larger than that of the global component. This was confirmed by the observation that turning off numerical diffusion from the first cell near the wall removes this inflexion point. The global numerical diffusion was

negligible in those tests, but the local numerical diffusion was significantly larger than that of the viscous diffusion. This removal of numerical diffusion eliminates the interference between the guard-cell values and the flux limiter by removing the dependency of numerical diffusion on the guard-cell values. In this note, this process is done by enforcing

$$\begin{aligned}\mu_{j=\frac{1}{2}}^f &= 0, \\ \nu_{j=\frac{1}{2}}^f &= 0,\end{aligned}\tag{13}$$

and

$$\begin{aligned}\mu_{j=\frac{3}{2}}^f &= 0, \\ \nu_{j=\frac{3}{2}}^f &= 0,\end{aligned}\tag{14}$$

where $j = \frac{1}{2}$ is the wall surface.

For an adiabatic wall, guard-cell values evaluated by equation (11) work well for most conditions, but oscillations arise if the temporal variation of the density at the wall is very large. This occurs, for instance, in a simulation of a compressible boundary layer, where a solid plate is suddenly placed in a high-speed uniform flow. We have found that these oscillations can be controlled by turning off numerical diffusion at the first cell near the wall. Thus, the interference between the guard-cell values and the flux limiter is also responsible for this numerical instability.

Besides turning off numerical diffusion at the first cell near the wall, the instability can be controlled by using an initial condition that ensues a gradual transition, or by adding numerical diffusion to the momentum equation (8) at an adiabatic wall. The viscosity in equation (8) for the latter approach has a numerical portion,

$$\mu_{num} = \frac{1 - D_c|_w}{6} \frac{\Delta y^2}{\Delta t},\tag{15}$$

where $D_c|_w$ is the coefficient used for the momentum equation at the wall, Δy is the grid size in the normal direction, and Δt is the time step. The total viscosity in equation (8) is $\mu = \mu_{phys} + \mu_{num}$, where μ_{phys} is the physical viscosity. Equation (15) is very similar to the numerical viscosity derived for the global numerical diffusion in FCT [8]. This numerical

diffusion, however, is only applied to the momentum equation at the wall and is needed only when temporal variations of the density are large. It can be gradually decreased when temporal variations at the wall become small.

4. Numerical Results

A boundary-layer flow with a Mach number of 2.4 is chosen for testing the boundary conditions at the wall. Thermal conditions of an adiabatic and an isothermal wall are tested. Figure 1 shows the schematic diagram of the computational set-up, and the computation parameters are summarized in Table 1. The quantity M_∞ is the free-stream Mach number, and Re_{ref} is the Reynolds number per centimeter. The viscosity is calculated by Sutherland's theory [10]. A flat plate with a length of 12 cm is placed at 1 cm away from the inflow plane. A slip-wall boundary condition is used for the section between the inflow plane and the flat plate. Since the Reynolds number at the end of the plate is approximately 4×10^5 , the flow is assumed laminar. The Courant number $CFL = 0.22$ and the coefficient $D_c = 0.999$ is used for all simulations. Results for two types of thermal conditions are given below.

Two approaches are tested for the simulation with an adiabatic wall. These approaches include adding extra numerical diffusion to the momentum equation (8) and turning off numerical diffusion at the first cell near the wall. Two types of $D_c|_w$ are used to test the effect of the added numerical diffusion on the final results. One is a constant value, $D_c|_w = 0.9$, which introduces a numerical viscosity roughly equal to seven times the physical viscosity near the wall. Another one is a gradually decreasing numerical viscosity, which is done by using $D_c|_w = \min[1.0, 0.9 + (1 - 0.9)t/t_c]$, in which t is the simulation time and t_c is the time when the temporal variation of the density near the wall becomes small. No global numerical diffusion is added in equation (8) after the time t_c .

Figure 2a shows both the theoretical predictions and experimental measurements of the streamwise velocity extracted from reference [10] for an adiabatic, laminar boundary layer

with $M_\infty = 2.4$. The momentum thickness δ_2 is calculated as

$$\delta_2 = \int_0^\infty \frac{\rho u}{\rho_\infty U_\infty} \left(1 - \frac{u}{U_\infty}\right) dy. \quad (16)$$

Figures 2b-2d show the current numerical results of the streamwise velocity at $x = 7\text{ cm}$, 9 cm , and 11 cm , along with the theoretical prediction extracted from Ref. [10]. The Reynolds numbers of these locations are roughly 2.4×10^5 , 3.1×10^5 , and 3.7×10^5 , respectively. Figure 2b shows the result using a constant $D_c|_W = 0.9$, and Figure 2c shows the result of a decreasing numerical viscosity that uses $D_c|_W = \min[1.0, 0.9 + (1 - 0.9)t/t_c]$. Finally, Figure 2d presents the result when numerical diffusion is turned off at the first cell near the wall. All the results agree well with the theoretical prediction. In addition, the temperature and density profiles from these three simulations agree very well with each other, as shown in Figures 3a and 3b. This good agreement indicates that numerical results are not sensitive to the amount of numerical diffusion added to the momentum equation (8) in this supersonic boundary-layer flow. Furthermore, the temperature ratios, $\frac{T_W}{T_\infty}$, predicted by these simulations are shown in Figure 4, along with the prediction given by Schlichting [10] :

$$T_W \approx T_\infty \left(1 + \sqrt{Pr} \frac{\gamma - 1}{2} M_\infty^2\right). \quad (17)$$

The comparison is good in regions away from the leading edge. There are some differences, however, in the leading edge region, where a much finer resolution is needed to resolve the variations there.

Figures 5a to 5c are the streamwise velocity, temperature, and density at $x = 9\text{ cm}$ for the boundary layer with an isothermal wall, where the temperature is set to the ambient value. The grid size in the y direction is half of that used in the adiabatic case because gradients of the density and temperature near the wall are steeper than those with an adiabatic wall. Numerical results obtained by turning off numerical diffusion at the first cell near the wall agree very well with those obtained by using equation (12). The peak values of the temperature and the density occur roughly at $2.8\delta_2$.

4. Conclusions

The implementation of boundary conditions at the wall in FCT has been studied. We have found that direct extrapolation from the interior points to evaluate the wall pressure introduce instability when the temporal variation of the density at the wall is not small. In this case, the continuity equation and the given thermal conditions at the wall can be used to evaluate the wall pressure. Since viscous diffusion can be evaluated from the flow variables at interior points and those at the wall, the guard-cell values only affect numerical diffusion and the performance of the flux limiter near a stationary no-slip wall.

It is found that the interference between the guard-cell values and the flux limiter can either affect the numerical results near the wall or introduce instability. Several approaches have been proposed to resolve this problem. These approaches include turning off numerical diffusion at the first cell near the wall to avoid the interference, or adding numerical diffusion to the momentum equation at the wall when an adiabatic wall is considered. We have found that these approaches work well for a compressible, supersonic boundary layer, and the final results are not sensitive to the amount of numerical diffusion added in the momentum equation at the wall in a supersonic boundary-layer flow.

5. Acknowledgments

This work was sponsored by the Office of Naval Research, and computational resources were provided by the Laboratory for Computational Physics and Fluid Dynamics at NRL. We would like to thank Prof. Bakhtier Farouk and his students for their work in applying approaches shown in this note to simulating thermoacoustic phenomena.

References

- [1] Y.S. Weber, E.S. Oran, and J.P. Boris, The numerical simulation of shock bifurcation near the end wall of a shock tube, *Phys. Fluids* **7** (1995) 10.
- [2] X.N. Saint-Martin-Tillet and E.S. Oran, private communication.
- [3] T. J. Poinsot, and S. K. Lele (1992), Boundary Conditions for Direct Simulations of Compressible Viscous Flows, *J. Comput. Phys.* **101** (1992) 104.
- [4] F.F. Grinsterin, Open Boundary Conditions in the Simulation of Subsonic Turbulent Shear Flows, *J. Comput. Phys.* **115** (1994) 43.
- [5] J.P. Boris and D.L. Book, Flux-Corrected Transport I: SHASTA A Fluid Transport Algorithm That Works, *J. Comput. Phys.* **11** (1973) 38.
- [6] J.P. Boris, A.M. Landsberg, E.S. Oran, J.H. Gardner, LCPFCT – A Flux Corrected Transport Algorithm for Solving Generalized Continuity Equations, NRL Memorandum Report 6410-93-7192, Naval Research Laboratory, Washington, DC, 1993.
- [7] J.P. Boris, D.L. Book, Solution of the continuity equation by the method of flux-corrected transport, *Methods in Computational Physics* **16** (1976) 85.
- [8] J. Liu, E.S. Oran, C.R. Kaplan, Numerical diffusion in the FCT algorithm, revisited, *J. Comput. Phys.* **208** (2005) 416.
- [9] E.S. Oran and J.P. Boris, *Numerical Simulation of Reactive Flow*, Cambridge University Press, 2001.
- [10] H. Schlichting, *Boundary-layer Theory*, McGraw-Hill, New York, 1987.
- [11] R.M. O'Donnell, Experimental investigation at Mach number of 2.41 of average skin friction coefficients and velocity profiles for laminar and turbulent boundary layers assessment of probe effect. NACA TN 3122 (1954).

- [12] D.R. Chapman and M.W. Rubesin, Temperature and velocity profiles in the compressible laminar boundary layer with arbitrary distribution of surface temperature. JAS 16, 547-565 (1949).

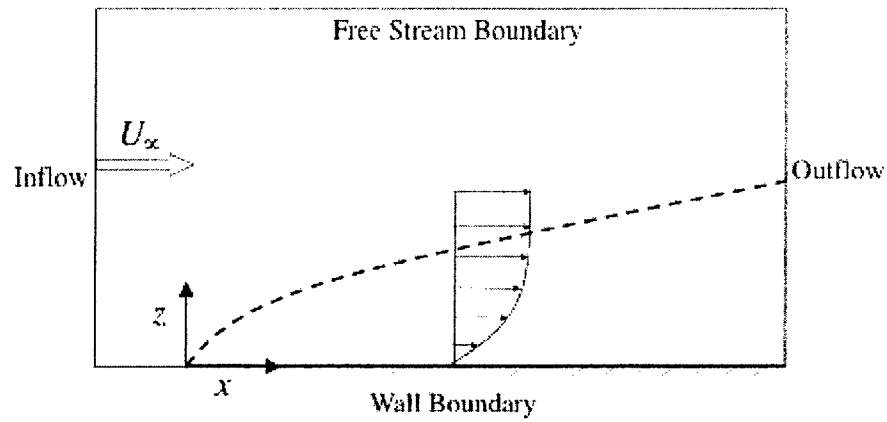


Figure 1. The schematic diagram of a boundary-layer flow on a flat plate. U_∞ is the inflow velocity. Free stream boundary: zero-gradient conditions. Inflow boundary: supersonic inflow conditions. Outflow boundary: supersonic outflow conditions. Wall boundary: no-slip conditions.

Table 1

Parameters for boundary-layer flow simulations on a flat plate

M_∞	Δx	Δy	Y_{\max}	L	Re_{ref}	Pr	T_∞	P_∞
2.4	0.1 cm	0.005 cm	0.5 cm	12 cm	34047	0.72	1447 K	0.41 atm

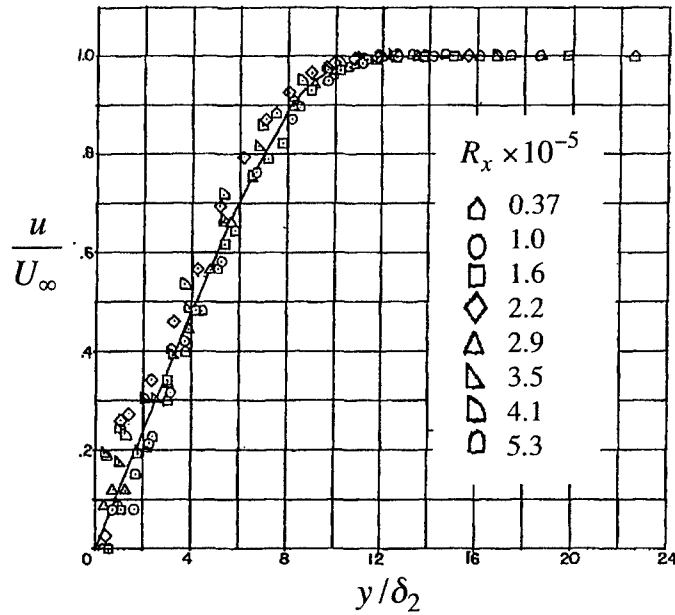


Figure 2a. Streamwise velocity profiles in an adiabatic, laminar boundary layer with $M_\infty = 2.41$. Symbols: measurements after R.M. O'Donnell [11]. Solid line: compressible theory prediction from Ref. [12]. Quantity δ_2 is the momentum thickness of the boundary layer. Dashed line: incompressible theory prediction.

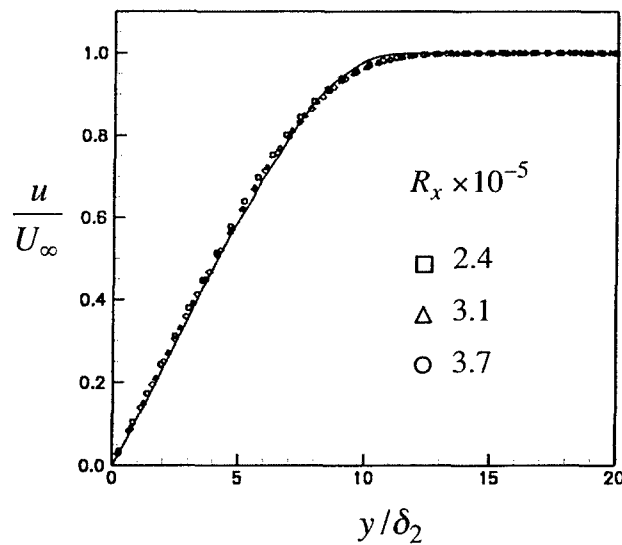


Figure 2b. Streamwise velocity profiles at $x = 7$ cm, 9 cm, and 11 cm with the adiabatic wall condition. Symbols: numerical results of $D_c|_W = 0.9$. Solid line: compressible theory prediction from Ref. [12]. Quantity δ_2 is the momentum thickness of the boundary layer.

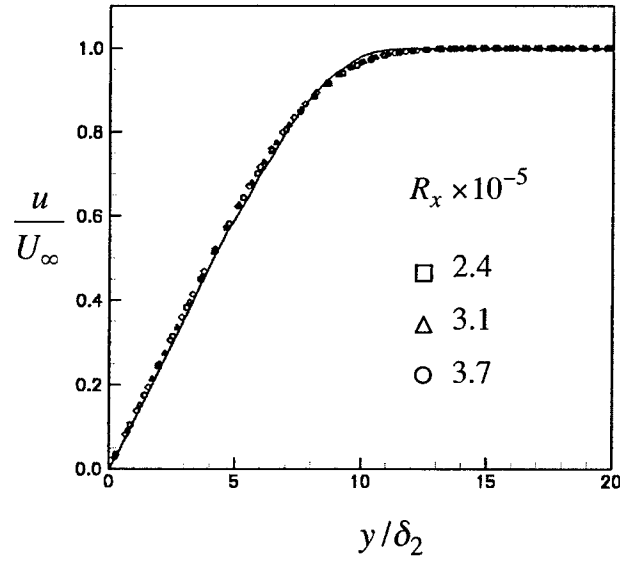


Figure 2c. Streamwise velocity profiles at $x = 7$ cm, 9 cm, and 11 cm with the adiabatic wall condition. Symbols: numerical results of $D_c|_w = \min[1.0, 0.9 + (1.0 - 0.9)t/t_c]$. Solid line: compressible theory prediction from Ref. [12]. Quantity δ_2 is the momentum thickness of the boundary layer.

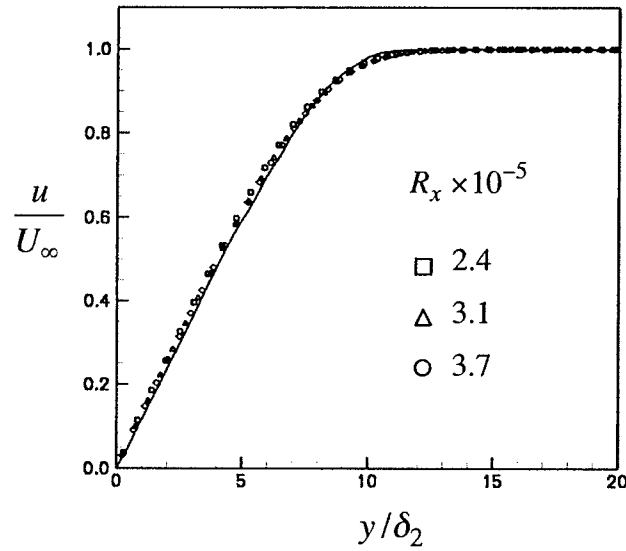


Figure 2d. Streamwise velocity profiles at $x = 7$ cm, 9 cm, and 11 cm with the adiabatic wall condition. Symbols: numerical results of turning off numerical diffusion from the first cell near the wall. Solid line: compressible theory prediction from Ref. [12]. Quantity δ_2 is the momentum thickness of the boundary layer.

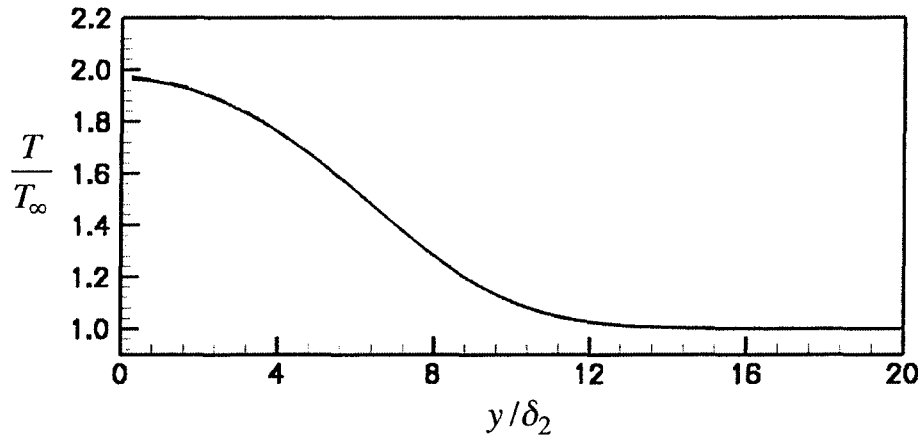


Figure 3a. Temperature profiles at $x = 9$ cm in an adiabatic, laminar boundary layer with $M_\infty = 2.4$. Solid line: tuning off numerical diffusion from the first cell near the wall. Dashed line: adding numerical diffusion in momentum equation (8) with a decreasing $D_c|_W = \min[1.0, 0.9 + (1.0 - 0.9)t/t_c]$. Dotted line: adding numerical diffusion in momentum equation (8) with a constant $D_c|_W = 0.9$.

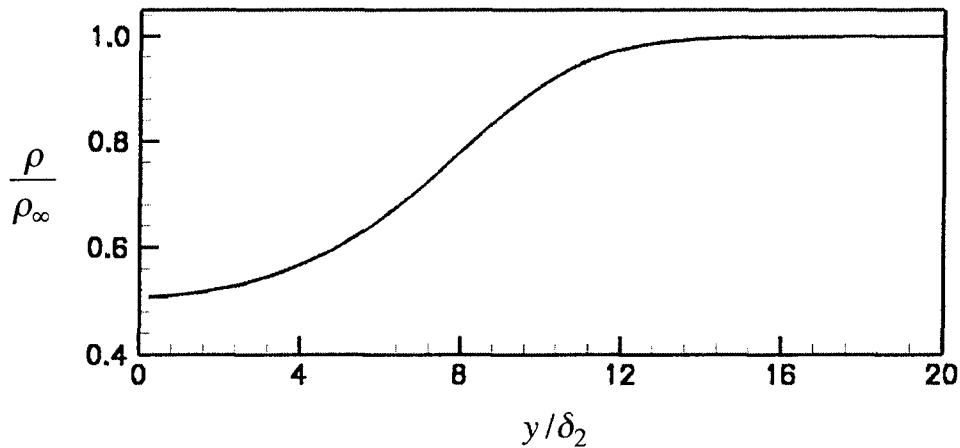


Figure 3b. Density profiles at $x = 9$ cm in an adiabatic, laminar boundary layer with $M_\infty = 2.4$. Solid line: tuning off numerical diffusion from the first cell near the wall. Dashed line: adding numerical diffusion in momentum equation (8) with a decreasing $D_c|_W = \min[1.0, 0.9 + (1.0 - 0.9)t/t_c]$. Dotted line: adding numerical diffusion in momentum equation (8) with a constant $D_c|_W = 0.9$.

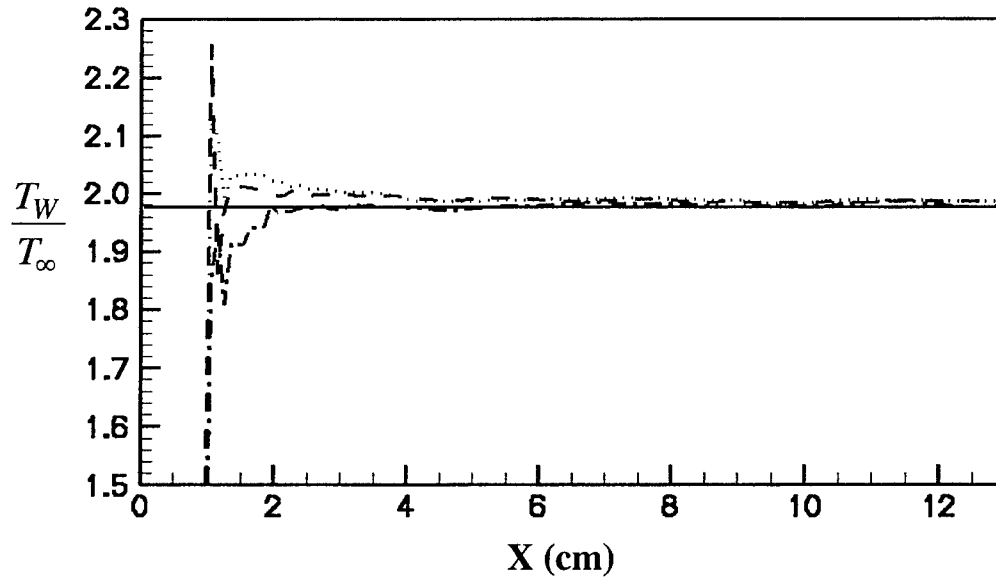


Figure 4a. Temperature distribution along the wall in an adiabatic, laminar boundary layer with $M_\infty = 2.4$. Solid line: prediction from equation (17) [10]. Dashed line: adding numerical diffusion in momentum equation (8) with a decreasing $D_c|_W = \min[1.0, 0.9 + (1.0 - 0.9)t/t_c]$. Dotted line: adding numerical diffusion in momentum equation (8) with a constant $D_c|_W = 0.9$. Dashed-Dotted line: tuning off numerical diffusion from the first cell near the wall.

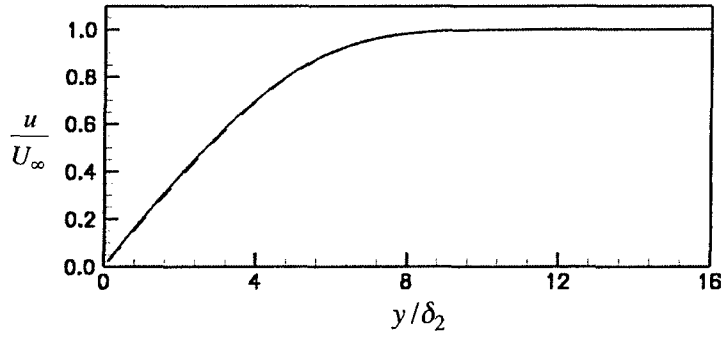


Figure 5a. Streamwise velocity profiles at $x = 9$ cm in an isothermal, laminar boundary layer with $M_\infty = 2.4$ ($T_W = T_\infty$). Solid line: tuning off numerical diffusion from the first cell near the wall. Dashed line: using equation (12).

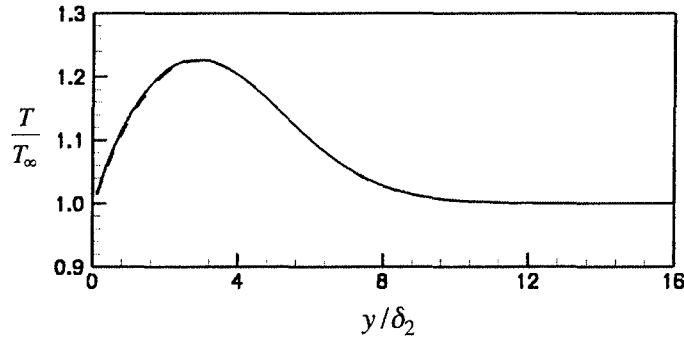


Figure 5b. Temperature profiles at $x = 9$ cm in an isothermal, laminar boundary layer with $M_\infty = 2.4$ ($T_W = T_\infty$). Solid line: tuning off numerical diffusion from the first cell near the wall. Dashed line: using equation (12).

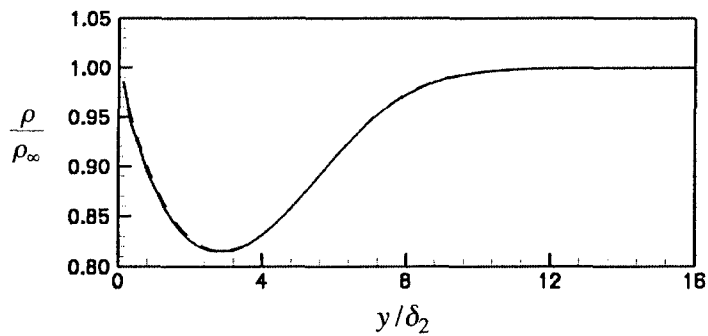


Figure 5c. Density profiles at $x = 9$ cm in an isothermal, laminar boundary layer with $M_\infty = 2.4$ ($T_W = T_\infty$). Solid line: tuning off numerical diffusion from the first cell near the wall. Dashed line: using equation (12).